Magnetic Shielding, Aromaticity, Antiaromaticity and Bonding in the Low-Lying Electronic States of S_2N_2

Peter B. Karadakov*[a], Muntadar A. H. Al-Yassiri[a] and David L. Cooper[b]

Abstract: Aromaticity, antiaromaticity and chemical bonding in the ground (S_0), first singlet excited (S_1) and lowest triplet (T_1) electronic states of disulfur dinitride, S_2N_2, are investigated by analysing isotropic magnetic shielding, $\sigma_{iso}(\mathbf{r})$, in the space surrounding the molecule for each electronic state. The $\sigma_{iso}(\mathbf{r})$ values are calculated using state-optimized CASSCF/cc-pVTZ wavefunctions with 22 electrons in 16 orbitals constructed from gauge-including atomic orbitals (GIAOs). The S_1 and T_1 electronic states are confirmed as $1\,^1A_u$ and $1\,^3B_{3u}$, respectively, through linear response CC3/aug-cc-pVTZ calculations of the vertical excitation energies for eight singlet (S_1–S_8) and eight triplet (T_1–T_8) electronic states. The aromaticities of S_0, S_1 and T_1 are also assessed using additional magnetic criteria including nucleus-independent chemical shifts (NICS) and magnetic susceptibilities calculated at several levels of theory, the highest of which are CCSDT-GIAO/cc-pVTZ for S_0 and CASSCF(22,16)-GIAO/aug-cc-pVQZ for S_1 and T_1. The results strongly suggest that the S_0 electronic ground state of S_2N_2 is aromatic, but less so than is the electronic ground state of benzene, S_1 is profoundly antiaromatic, to an extent that removes any bonding interactions that would keep the atoms together, and T_1 is also antiaromatic, but its antiaromaticity is more moderate and similar to that observed in the electronic ground state of square cyclobutadiene. S_2N_2 is the first example of an inorganic ring for which theory predicts substantial changes in aromaticity upon vertical transition from the ground state to the first singlet excited or lowest triplet electronic states.

Introduction

Disulfur dinitride, S_2N_2, was most probably first generated but went unnoticed in an experiment carried out by O. C. M. Davis at University College, Bristol: Heating of $S_4N_4{\cdot}SbCl_5$ resulted in the formation

[a] *Dr. P. B. Karadakov, Muntadar Al-Yassiri*
Department of Chemistry, University of York
Heslington, York YO10 5DD (UK)
E-mail: peter.karadakov@york.ac.uk

[b] *David L. Cooper*
Department of Chemistry, University of Liverpool
Liverpool L69 7ZD (UK)

of a blue substance, identified later as the $(SN)_x$ polymer. Burt described Davis's experiment in a 1910 paper[1] in which he reported that passing S_4N_4 vapour over a silver gauze or quartz wool produced blue films or bronze-coloured crystals and suggested "that the immediate precursor of the blue sulphide of nitrogen is a gas or very volatile liquid at the ordinary temperature". These observations were explained by Goehring and Voigt[2] who established that the thermal decomposition of S_4N_4 yields S_2N_2, a white volatile crystalline solid, which polymerizes to $(SN)_x$.

Except for being a precursor to $(SN)_x$, a polymer exhibiting metallic conductivity[3] and superconductivity[5], S_2N_2 is of relatively little experimental importance. However, the nature of bonding in this four-membered inorganic ring with 6π electrons and its level of aromaticity have been the subject of numerous theoretical studies.

One of the popular models for the electronic structure of S_2N_2, shown in **1**, can be traced back to an Edmiston-Ruedenberg[6] localization of the MOs from a CNDO/2 spin-restricted Hartree-Fock (RHF) calculation carried out by Adkins and Turner[7]. They obtained LMOs corresponding to two three-centre π orbitals localized mostly on the nitrogen atoms, a sulfur-sulfur non-bonding π orbital, four S–N σ bonds and four σ lone pairs (one on each atom).

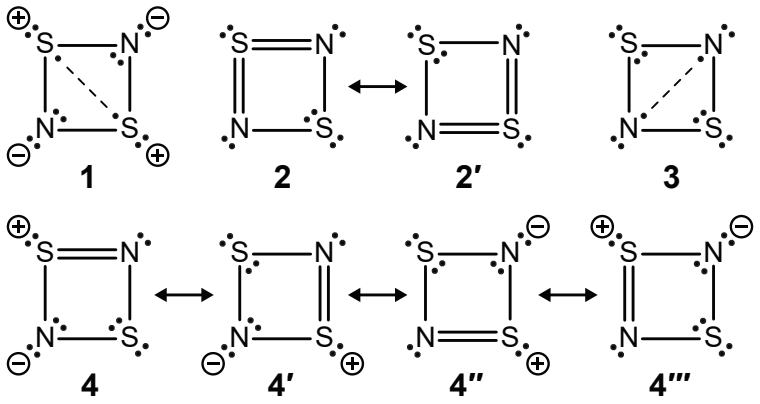

Another model, featuring on the pages of a well-known inorganic chemistry textbook[8], was suggested by Findlay *et al.*[9] on the basis of a Foster-Boys[10] localization of the MOs from an *ab initio* RHF calculation in a "better than double ζ" basis set. The eleven valence-shell LMOs were found to describe four "bent" bonds which attach one of the sulfur atoms to the neighbouring nitrogen atoms by two double bonds, two S–N σ bonds involving the second sulfur atom, which carries a π lone pair, and four σ lone pairs, similar to those in **1**. As the resulting bonding scheme **2**, on its own, would be of broken symmetry, it is thought to be in resonance with **2′**. The initial source of **3** was an INDO valence bond (VB) calculation involving all ten VB structures arising from distributing six electrons amongst the four sulfur $3p_\pi$ and nitrogen $2p_\pi$ orbitals, carried out by Fujimoto and Yokoyama[11], in which the dominant VB structure turned out to be a singlet diradical with a diagonal singlet pair involving the two nitrogen $2p_\pi$ orbitals.

Calculations with a π-space spin-coupled (SC) wavefunction, which is the most general wavefunction utilizing a single product of non-orthogonal MOs, lend support to a singlet diradical version of **1**[12], similar to the Adkins and Turner model[7]; the important new element is that two of the six singly-occupied active π orbitals are found to resemble closely S($3p_\pi$) AOs, with spins coupled to a singlet. On the other hand, a series of VB studies performed by Harcourt and coworkers (see reference [13] and references therein) provide backing for the alternative singlet diradical scheme **3**. Thorsteinsson and Cooper obtained three individually optimized π-space CASSCF(6,6) ("6 electrons in 6 orbitals" complete-active-space self-consistent field) wavefunctions corresponding to schemes **1**, **2** and **3**[14]. According to their results, **1** is slightly lower in energy than **2**, by just over 0.5 millihartree, while **3** is significantly higher, 8.6 millihartree above **1**. CASVB transformations of these CASSCF wavefunctions provided π-space SC-like descriptions of the three bonding schemes, reproducing closely, in the case of **1**, the SC picture from reference [12]. Subsequent breathing orbital VB (BOVB) calculations, carried out by Braïda *et al.*[15], produced wavefunctions in which the VB structure with the largest weight turned out to be **3**, followed by each of the four symmetry-equivalent covalent structures **4**–**4‴**, with **1** coming only sixth in importance. However, it is appropriate to highlight a problem with VB wavefunctions constructed from non-orthogonal structures: There is no unambiguous way of assigning weights to individual structures. The standard Chirgwin-Coulson approach[16] is based on an obvious but arbitrary partitioning of the normalization integral and may produce negative weights, as well as weights larger than one. Alternative weighting schemes have been shown to yield very different results in some instances[17] and they could, in principle, place more emphasis on **1** at the expense of other structures. Interestingly, Braïda *et al.* showed[15] that, if working in a minimal basis set, the expansion of the π-space part of the SC wavefunction for S_2N_2 from reference [12] in terms of VB structures constructed from AOs can be reasonably well approximated by a single structure corresponding to **3**. This is an indication that the lowest-energy SC[12,14] and VB[13,15] wavefunctions for S_2N_2 have much in common and the preferred interpretation is down to some extent to personal choice. In very recent work, Penotti *et al.*[4] projected various SC wavefunctions onto the basis of BOVB structures used by Braïda *et al.*[15], plus an orthogonal complement. They consistently found structure **3** to be more important than **1** but the largest contribution (approaching 60% of the total wavefunction) could be associated with the symmetry-determined linear combination of the four symmetry-equivalent structures **4**–**4‴**. Irrespective of disagreements about the positioning of the radical sites, all of the VB studies of S_2N_2 suggest a significant degree of singlet diradical character in the electronic ground state.

Other theoretical studies provide evidence both in favour and against the idea that S_2N_2 should be considered as a singlet diradical. Tuononen *et al.*[18] showed that the RHF wavefunction for S_2N_2 is non-singlet unstable: There is a lower-energy broken-symmetry spin-unrestricted HF (UHF) wavefunction,

consistent with singlet diradical character. On the other hand, three density functional theory (DFT) methods provide spin-restricted solutions that are non-singlet stable: BPW91 and B3PW91 calculations were reported in reference [18], and a B3LYP calculation was reported in reference [19]. In a subsequent paper[20], Tuononen *et al.* argued that whereas the non-singlet instability of a RHF wavefunction is an indication of its inadequate quality, which can be linked to singlet diradical character, the analogous stability analysis of a spin-restricted DFT solution tests only the ability of a certain exchange-correlation potential to describe the electron density of a singlet system using a closed-shell Slater determinant of Kohn-Sham orbitals. The same authors also compared the so-called fraction of diradical character[21,22] for S_2N_2, 6%, calculated from a CASSCF(22,16) wavefunction, to the corresponding fraction for ozone, 26%, based on a CASSCF(18,12) wavefunction[18]. While 6% is not an indication of significant diradical character, an additional analysis of their CASSCF(22,16) wavefunction for S_2N_2 in terms of Lewis-type VB structures corresponding to **1** and **3** using idealized p_π orbitals showed that these diradical structures account for 14% and 34% of the wavefunction, respectively, or 48%, when taken together.

The absence of a spin-unrestricted DFT solution was just one of the factors that led Head-Gordon *et al.*[19] to the conclusion that the diradical character of S_2N_2 is not significant. They also considered the B3LYP HOMO-LUMO gap (which was found to be much larger than the corresponding gaps in diradicaloid species of the same size), the large singlet-triplet gap, and the occupation numbers of the antibonding orbitals in VOD(22,22) (valence space optimized doubles with 22 electrons in 22 orbitals) and in CASSCF(6,4) wavefunctions, which turned out to be similar to the corresponding VOD(30,30) results for benzene. According to Head-Gordon *et al.*[19], structural and magnetic criteria suggest that S_2N_2 is aromatic: It is a planar four-membered ring with equal S–N bond lengths, intermediate between a single and a double bond, and exhibits a sizeable negative π CMO-NICS(0) (canonical molecular orbital decomposition analysis of nucleus-independent chemical shifts[23,24]) value of -26.2 ppm (at the PW91-GIAO/IGLO-III level, DFT with gauge-including atomic orbitals). On the other hand, the aromatic stabilization energy of S_2N_2 obtained by Head-Gordon *et al.*[19] is small, 6.5 kcal mol^{-1}, which was thought to be an indication that although the six π electrons make this molecule compliant with Hückel's $4n+2$ rule, the higher, nearly degenerate set of π orbitals do not contribute significantly to the bonding. Accordingly, they argued that S_2N_2 should be viewed as an aromatic system with 2π electrons, with S–N bond order close to 1.25. A bond order of this magnitude is consistent with the observation that the bond length in S_2N_2 is between those of typical S–N single and double bonds[19]. Interestingly, the NICS(0) value of 5.6 ppm for S_2N_2 reported in reference [19] indicates antiaromaticity, but this positive value was attributed to large σ orbital contributions not relevant for aromaticity. Braïda *et al.*[15] argued that the diradical character of S_2N_2 can co-exist with aromaticity and suggested that its π elec-

tron system features collective electron flow along a loop connecting **1**, **3** and **4**–**4**‴ through successive one-electron transfers.

Electronic excited states of S_2N_2 have been calculated at several levels of theory, including configuration interaction (CI)[25], multi-reference CI (MRCI)[26], time-dependent DFT (TDDFT)[20,27], equations-of-motion coupled-cluster with single and double excitations (EOM-CCSD), state-averaged CASSCF(22, 16) and CASPT2(22,16) (second-order perturbation theory with a state-averaged CASSCF reference)[20]. Tuononen *et al.*[20] also carried out time-dependent HF (TDDHF) and second-order polarization propagator approximation (SOPPA) excited state energy calculations but did not report the results because they were found to be unsatisfactory. The experimental UV absorption spectrum of S_2N_2 features a broad band with vibrational fine structure between 4.49–5.85 eV, which could arise from two overlapping bands centred at approximately 5.03 and 4.97 eV, the second of which is slightly lower in intensity[27]. The only electric dipole allowed transitions from the $1\,^1A_{1g}$ ground state are to singlet excited states of B_{1u}, B_{2u} and B_{3u} symmetries. Calculated oscillator strengths[20,26,27] show that the intensity of the transition to the $1\,^1B_{2u}$ state is much higher than that to the $1\,^1B_{3u}$ state, while the intensity of the transition to the $1\,^1B_{1u}$ state is negligibly low. The most thorough excited state calculations on S_2N_2 available to date, including time-dependent DFT (TDPBEPBE and TDPBE0), EOM-CCSD and state-averaged CASSCF(22,16) and CASPT2(22,16) in the cc-pVTZ and aug-cc-pVTZ basis sets[20], predict that the $1\,^1B_{2u}$ state is lower in energy than the $1\,^1B_{3u}$ state, although the reverse ordering of these states that is observed in some TDDFT results[27] would fit better with the shape of the broad band in the experimental absorption spectrum. CASPT2(22,16) is found to underestimate the $1\,^1B_{2u}$ and $1\,^1B_{3u}$ excitation energies, while TDPBEPBE, TDPBE0, EOM-CCSD and CASSCF(22,16) are found to overestimate these energies, with CASPT2(22,16), TDPBEPBE and TDPBE0 coming closer to the *ca.* 5 eV value suggested by the experimental absorption spectrum than do EOM-CCSD and CASSCF(22,16)[20].

In this paper we study bonding and aromaticity in the ground, first singlet excited and lowest triplet electronic states of S_2N_2 by analysing the changes in the off-nucleus magnetic shielding tensor, $\boldsymbol{\sigma}(\mathbf{r})$, within the space surrounding the molecule. Previous research on carbon-carbon bonds[28,29] showed that the off-nucleus isotropic magnetic shielding, $\sigma_{\rm iso}(\mathbf{r}) = \frac{1}{3}[\sigma_{xx}(\mathbf{r}) + \sigma_{yy}(\mathbf{r}) + \sigma_{zz}(\mathbf{r})]$, is capable of exposing the differences between carbon-carbon bonds of different multiplicities in much greater detail than is achievable using the total electronic density. One of our aims is to establish whether the variations in $\sigma_{\rm iso}(\mathbf{r})$ provide similar insights into the nature of the S–N bond in S_2N_2. While a popular approach for investigating aromaticity, namely the calculation of single-point NICS(0) indices, has already been applied to S_2N_2[19], the examination of $\sigma_{\rm iso}(\mathbf{r})$ isosurfaces and contour plots can provide somewhat more detailed and, arguably, more reliable information about aromaticity and its effect on chemical

bonding[30]. The large volume of additional information that is required to represent the off-nucleus magnetic isotropic shielding as a function of position resolves some important criticisms towards single-point NICS, such as the arbitrariness in the choice of the locations at which such quantities are calculated (NICS can exhibit strong positional dependence and, in certain situations, the standard choices can be inappropriate, see *e.g.* references [31] and [32]) and the fact that a single number might not be sufficient to characterize all aspects of aromatic behaviour, illustrated by the observation that different ring current maps can produce nearly indistinguishable single-point NICS values[33,34].

There has been substantial recent interest in aromaticity and antiaromaticity reversals upon transition from the ground electronic state to a higher electronic state[35–37]. The first and better-known reversal of this type is associated with Baird's rule[38], according to which the familiar $4n + 2$ and $4n$ rules for ground-state aromaticity in cyclic conjugated hydrocarbons are switched over in their lowest triplet states: rings with $4n$ π electrons become aromatic while those with $4n + 2$ π electrons end up as being antiaromatic. The second type of excited state aromaticity reversal is an analogous phenomenon associated with the lowest singlet excited states[39–41]. We show that S_2N_2 is the first example of an inorganic ring which can be expected to exhibit substantial changes in aromaticity upon transition from the singlet ground electronic state to the first singlet excited or lowest triplet electronic states.

Computational Procedure

In all calculations on S_2N_2 reported in this paper we used the D_{2h} semi-experimental equilibrium geometry established by Perrin *et al.*[42], with $R(\mathrm{SN}) = 1.64182$ Å and $\angle(\mathrm{NSN}) = 91.0716°$, in a coordinate system that places the nitrogen atoms at positions $(\pm 1.171748, 0.0, 0.0)$, and the sulfur atoms at positions $(0.0, \pm 1.150035, 0.0)$, respectively (all coordinates in Å).

In order to obtain detailed contour plots describing changes in isotropic shielding that can be associated with chemical bonding and aromaticity in the regions of space surrounding the ground (S_0), first singlet excited (S_1) and lowest triplet (T_1) electronic states of S_2N_2, the off-nucleus isotropic magnetic shielding $\sigma_{\mathrm{iso}}(\mathbf{r})$ for each electronic state was evaluated at regular two-dimensional grids of points with spacing of 0.05 Å in five planes: Two horizontal planes, including the molecular plane and a plane parallel to the molecular plane and 1 Å above it, as well as three vertical planes perpendicular to the molecular plane, with one passing through the two nitrogen atoms, one through the two sulfur atoms, and the third one through one of the S–N bonds. For the purposes of comparison, $\sigma_{\mathrm{iso}}(\mathbf{r})$ calculations were also carried out for the electronic ground state of benzene at the D_{6h} geometry with $R(\mathrm{CC}) = 1.3964$ Å and $R(\mathrm{CH}) = 1.0831$ Å that was used in references [39, 41]. In this case, the regular grids of points with spacing of 0.05 Å were placed in three planes: Two horizontal planes, defined as those for S_2N_2, and a vertical plane passing through one of the C–C bonds. In order to reduce computational effort,

$\sigma_{\rm iso}(\mathbf{r})$ values were calculated only at symmetry-unique grid points.

The $\sigma_{\rm iso}(\mathbf{r})$ calculations for the low-lying electronic states of S_2N_2 were carried out using state-optimized CASSCF-GIAO wavefunctions. We selected a "22 in 16" active space analogous to that adopted by Tuononen *et al.*[18,20] including, as an initial guess, the eleven highest occupied and five lowest virtual RHF orbitals. Off-nucleus isotropic magnetic shielding values for the electronic ground state of benzene were obtained using the usual π-space CASSCF(6,6)-GIAO wavefunction. All of these calculations were carried with the standard cc-pVTZ basis set.

As a consequence of the decision to use ground-state geometries for all of the electronic states studied in this paper, the comparisons between the properties of the electronic states of S_2N_2 are in the context of vertical excitations. In line with previous work on NICS[39–41,43] and ring currents[44] in triplet systems, the CASSCF-GIAO isotropic shieldings in the lowest triplet electronic state of S_2N_2 reported in this paper include the contributions arising from the perturbation to the wavefunction only (often referred to as "orbital" contributions in single-determinant approaches). This choice is convenient for the purposes of the current study, as the values reported for a triplet state can be compared directly to those for singlet states. A more rigorous treatment would need to take into account the large terms associated with the interaction between the electronic spin angular momentum and the magnetic field[45,46].

Given that state-optimized CASSCF calculations account only for static electron correlation effects, they do not always reproduce the correct energy ordering of the electronic excited states. One example is provided by benzene[47], for which the order of the third (S_3) and fourth (S_4) singlet electronic excited states is reversed at the CASSCF level; getting these states in the correct order requires the inclusion of dynamic electron correlation effects, for example, through the use of CASPT2. As there is only very limited experimental information on the excitation energies from the ground electronic state to other low-lying electronic states of S_2N_2, we decided to obtain more reliable theoretical estimates of these energies through linear response calculations using two advanced coupled-cluster (CC) approaches, namely CC3 and CCSDR(3)[48,49], and we compare these results to those for state-optimized CASSCF(22,16) wavefunctions (in addition, CC3 provides intermediate CCSD results). For the CC3 and state-optimized CASSCF(22,16) calculations we used the cc-pVTZ and aug-cc-pVTZ basis sets, and for the CCSDR(3) calculations, the cc-pVTZ, cc-pVQZ, aug-cc-pVTZ and aug-cc-pVQZ basis sets.

In order to gain better understanding of the method and basis set dependence of the magnetic properties of the low-lying electronic states of S_2N_2, we carried out additional calculations of the sulfur and nitrogen isotropic shieldings, magnetic susceptibilities and the NICS(0), NICS(0)$_{zz}$, NICS(1) and NICS(1)$_{zz}$ aromaticity indices at several levels of theory: CASSCF(22,16)-GIAO with the cc-pVQZ, aug-cc-pVTZ and aug-cc-pVQZ basis sets for S_0, S_1 and T_1, and RHF-based HF-GIAO, MP2-GIAO, CCSD(T)-GIAO and CCSDT-GIAO, all with the cc-pVTZ basis, for the electronic ground state. Ad-

ditionally, the corresponding set of magnetic properties for the electronic ground state of benzene were evaluated at the CASSCF(6,6)-GIAO/aug-cc-pVTZ level.

All CASSCF-GIAO calculations were performed by means of the MCSCF-GIAO (multiconfigurational SCF with GIAOs) methodology introduced in references [50, 51] and implemented in the Dalton 2016.2 program package[52]. For all other GIAO calculations we used CFOUR[53]. The CC excited state calculations were carried out using Dalton 2016.2[52], which is capable of performing linear response CC3 for both singlet and triplet states, and CCSDR(3) for singlet states.

Results and Discussion

The vertical excitation energies from S_0 to the next eight singlet (S_1–S_8) and the eight lowest triplet (T_1–T_8) electronic states of S_2N_2 calculated at different levels of theory are shown in Table 1. Our results confirm the observation of Tuononen *et al.*[20] that all of the S_1–S_8 states and similarly all of the T_1–T_8 states for S_2N_2 belong to different irreducible representations of the D_{2h} point group. As $2\,^1A_g$ is of the same symmetry as the electronic ground state ($1\,^1A_g$), the state-optimized CASSCF(22,16) calculations for $2\,^1A_g$ used the second root of the corresponding CI problem.

Place Table 1 near here.

The CCSD/cc-pVTZ vertical excitation energies to singlet and triplet states included in Table 1 are in good agreement with the corresponding results reported by Tuononen *et al.*[20], with the differences most likely being due to the use of different ground-state S_2N_2 geometries. The state-optimized and state-averaged CASSCF(22,16)/cc-pVTZ results from this work and from reference [20], respectively, show more differences: In reference [20], the vertical excitation energies to $1\,^1B_{3u}$ and $1\,^1B_{2u}$ are identical, $1\,^1B_{1g}$ is lower in energy than $1\,^1B_{3g}$, and four of the triplet states, $1\,^3B_{2u}$, $1\,^3B_{1u}$, $1\,^3B_{2g}$ and $1\,^3A_u$, appear in an order different from that in Table 1.

The general trends for singlet states that are suggested by the results shown in Table 1 is that the use of a higher level of theory, in the sequence state-optimized CASSCF(22,16) – CCSD – CCSDR(3) – CC3, decreases the singlet vertical excitation energy, and so does, but to a smaller extent, the increase of the basis set size. State-optimized CASSCF(22,16) puts two pairs of states in a different order from the CC approaches, such that $1\,^1B_{1u}$ is lower in energy than $1\,^1A_u$ and $1\,^1B_{3u}$ is lower in energy than $1\,^1B_{2u}$. CCSD shows a single ordering difference from CCSDR(3) and CC3: $1\,^1B_{1u}$ is higher in energy than $1\,^1B_{2g}$. As all of the CC results suggest that the lowest singlet excited state (S_1) is $1\,^1A_u$, we use this state in the magnetic shielding analysis. The only notable irregularity in the results for triplet states is that CCSD switches the energy ordering of $1\,^3B_{1g}$ and $1\,^3B_{3g}$. All methods identify T_1 as $1\,^3B_{3u}$.

Place Tables 2 and 3 near here.

The sulfur and nitrogen isotropic shieldings in the S_0, S_1 and T_1 electronic states of S_2N_2, and the carbon and proton isotropic shieldings for the electronic ground state of benzene are shown in Table 2. This table includes also results for the isotropic magnetic susceptibilities, $\chi_{\rm iso} = \frac{1}{3}(\chi_{xx} + \chi_{yy} + \chi_{zz})$,

and out-of-plane components of the magnetic susceptibility tensor, χ_{zz}. In Table 3 we report the corresponding NICS(0), NICS(0)$_{zz}$, NICS(1) and NICS(1)$_{zz}$ values for the electronic states of S_2N_2 and benzene, which follow the standard definitions, NICS(0) = $-\sigma_{iso}$(at the ring centre)[54], NICS(0)$_{zz}$ = $-\sigma_{zz}$(at the ring centre)[55,56], NICS(1) = $-\sigma_{iso}$(at 1 Å above the ring centre)[23,57] and NICS(1)$_{zz}$ = $-\sigma_{zz}$(at 1 Å above the ring centre)[58]. The CASSCF-GIAO/cc-pVTZ shielding data included in Tables 2 and 3 were extracted from the calculations of isotropic shieldings at the horizontal grids of points for the respective electronic states of S_2N_2 and benzene.

The CASSCF(6,6)-GIAO results for benzene with the cc-pVTZ and aug-cc-pVTZ basis sets reported in Tables 2 and 3 show only insignificant deviations from those computed previously at the CASSCF(6,6)-GIAO/6-311++G(2d,2p) level[39]. This is an indication that the quality of the cc-pVTZ basis is adequate for the purposes of the current analysis.

The differences between some of the theoretical estimates of the electronic ground state sulfur and nitrogen isotropic shielding values for S_2N_2 are considerable (see Table 2). Clearly, the CASSCF(22,16)-GIAO, CCSD(T)-GIAO and CCSDT-GIAO results are in good agreement, especially so far as $\sigma_{iso}(^{15}N)$ is concerned. HF-GIAO significantly exaggerates the deshielding of both nuclei but at least keeps sulfur more shielded than nitrogen, in line with CASSCF(22,16)-GIAO, CCSD(T)-GIAO and CCSDT-GIAO, while the MP2-GIAO isotropic shieldings are not only considerably higher than those obtained with all other methods but also suggest that sulfur is less shielded than nitrogen. According to Tuononen *et al.*[20], while RHF and MP2 can provide reasonable geometries and qualitatively correct vibrational frequencies for S_2N_2 and similar chalcogen-nitrogen compounds, these methods do not properly take into account the singlet diradical character of the molecules and fail to predict second- or third-order properties such as IR intensities, Raman activities, and NMR chemical shifts. The nuclear shielding data reported in Table 2 lends further support to this view.

The results for the S_2N_2 electronic ground state isotropic magnetic susceptibility, χ_{iso}, and out-of-plane component of the magnetic susceptibility tensor, χ_{zz}, obtained at different levels of theory (see Table 2) are in reasonable agreement and they suggest that this state is aromatic, but considerably less so than is the electronic ground state of benzene. For comparison, the χ_{iso} and χ_{zz} values for the strongly antiaromatic electronic ground state of square cyclobutadiene at the CASSCF(4,4)/6-311++G(2d,2p) level have been reported as –12.20 ppm cm^3 mol^{-1} and 12.88 ppm cm^3 mol^{-1}, respectively[39].

The S_0 NICS(0) values for S_2N_2 obtained with the CASSCF(22,16)-GIAO, CCSD(T)-GIAO and CCSDT-GIAO methods (see Table 3) are all positive but considerably smaller than the PW91-GIAO/IGLO-III figure of 5.6 ppm reported in reference [19] which, incidentally, coincides with our MP2-GIAO/cc-pVTZ result. On the other hand, the HF-GIAO/cc-pVTZ S_0 NICS(0) value of –4.74 ppm is well into the aromatic region. However, the analysis of the nuclear shielding data for the electronic

ground state of S_2N_2 (*vide supra*) suggests that neither of the MP2-GIAO/cc-pVTZ and HF-GIAO/cc-pVTZ S_0 NICS(0) values is likely to be accurate. Judging by the more reliable CASSCF(22,16)-GIAO, CCSD(T)-GIAO and CCSDT-GIAO results, the NICS(0) aromaticity index classifies the electronic ground state of S_2N_2 as mostly non-aromatic.

The high positive values of the S_0 NICS$(0)_{zz}$ index obtained at all levels of theory arise as a consequence of the high shielding anisotropy at the centre of the ring and should not be viewed as an indication of antiaromaticity. For example, at the CASSCF(22,16)-GIAO/cc-pVTZ level the principal components of the magnetic shielding tensor at the ring centre are $\sigma_{xx}(0) = 16.87$ ppm, $\sigma_{yy}(0) = 43.96$ ppm and $\sigma_{zz}(0) = -63.81$ ppm, respectively.

The S_0 NICS(1) and NICS$(1)_{zz}$ values which, arguably, are more reliable aromaticity indices than NICS(0) and NICS$(0)_{zz}$, but do not appear to have been applied previously to the electronic ground state of S_2N_2, are both negative at all levels of theory and suggest aromatic character, albeit somewhat weaker than that of benzene (see Table 3).

The data in Tables 2 and 3 show clearly that the electronic structure of S_2N_2 undergoes profound changes upon vertical excitation from S_0 to S_1 or T_1. The magnetic properties of S_1 included in these tables exhibit pronounced basis set dependence and change significantly when calculated using basis sets larger than cc-pVTZ; even the aug-cc-pVQZ results could be far from basis set convergence. Without exception, the NICS values for S_1 show very substantial deshielding at and above the ring centre which can be interpreted as an indication not only of very strong antiaromaticity but also of pronounced structural instability: This could be associated with the well-known fact that S_2N_2 decomposes explosively when struck or heated above 30 °C[8]. Larger basis sets containing more diffuse functions make the ring centre and its surroundings less deshielded but the level of deshielding of this region of space remains very high even in the results obtained with the aug-cc-pVQZ basis.

The basis set dependence of the magnetic properties of T_1 is much less pronounced and the results obtained with the cc-pVTZ basis are sufficiently accurate for properties other than the sulfur and nitrogen nuclear shieldings. The NICS, $\chi_{\rm iso}$ and χ_{zz} values for T_1 are similar to those for the electronic ground state of an archetypal example of an antiaromatic system, namely square cyclobutadiene (*vide supra*).

The spatial variations in isotropic shielding, $\sigma_{\rm iso}(\mathbf{r})$, for the S_0, S_1 and T_1 electronic states of S_2N_2 states are illustrated through the contour plots shown in Figures 1–9. In order to facilitate comparisons, Figures 1–3 include corresponding contour plots for the electronic ground states of S_2N_2 and benzene. The levels in the $\sigma_{\rm iso}(\mathbf{r})$ contour plots in Figures 1–9 are selected as different consecutive subsets from a consecutive range of values including −800, −700, −500, −480(20)−80, −70(10)−10, −5, 0, 1, 5(5)40, 50, 60(20)180 (all in ppm). The minimum and maximum values for the subset used in each figure are specified in the respective figure caption.

Place Figures 1, 2 and 3 near here.

The comparison between the isotropic shielding contour plots for the electronic ground states of S_2N_2 and benzene in the respective molecular planes (see Figure 1) reveals high levels of similarity, especially around the S–N and C–C bonds. Figures 1–3 show clearly that both rings are surrounded by doughnut-shaped regions of increased shielding, familiar from previous shielding studies of benzene[30,41]. Inside these regions, $\sigma_{iso}(\mathbf{r})$ reaches 42.69 ppm along a S–N bond and 45.22 ppm along a C–C bond. The $\sigma_{iso}(\mathbf{r})$ contour plots in planes 1 Å above the respective molecular planes (see Figure 2) and in vertical planes through the S–N and C–C bonds (see Figure 3) show that the doughnut-shaped region in S_2N_2 is smaller than that in benzene, mainly because it extends a smaller distance above and below the molecular plane. Nevertheless, its size is still sufficient to suggest that S_2N_2 is aromatic in its electronic ground state, but less so than is benzene. The $\sigma_{iso}(\mathbf{r})$ contours outside the ring, next to the sulfur and nitrogen atoms in Figure 1(a), indicate that the lone pairs on these atoms make similar relatively minor contributions to the isotropic shielding in the molecular plane, but are more pronounced around the sulfur atoms.

The deshielded region in the centre of the S_2N_2 ring is very small, much smaller than that in the electronic ground state of square cyclobutadiene[30,41]. Vertically, it extends to only about 0.32 Å above and below the ring centre (see Figure 4). This deshielded region is a minor feature which might be due to a number of reasons; for example, the σ electrons in S_2N_2 could be engaged in a weak antiaromatic system competing with the aromatic system formed by the π electrons.

Place Figure 4 near here.

The differences between the aromaticities of the electronic ground states of S_2N_2 and benzene is illustrated particularly well by the isotropic shielding contour plots in the planes that are parallel to the respective molecular plane and 1 Å above it (see Figure 2). The contour plot for benzene in Figure 2(b) features a thick circular band of isotropic shielding values above 15 ppm which has no equivalent in the S_2N_2 contour plot in Figure 2(a); the S_2N_2 counterpart to a much thicker circular band of isotropic shielding values above 10 ppm in benzene are two relatively small symmetry-equivalent regions of increased shielding above the nitrogen atoms. The presence of these regions suggests that the nitrogen atoms make more pronounced contributions to the π system of S_2N_2 than do the sulfur atoms. This is in line with two of the electronic structure models from the Introduction, **1** and the resonance between structures **4**–**4**‴, according to which the nitrogen and sulfur atoms are negatively and positively charged, respectively. The charge distribution in S_2N_2 was discussed by Head-Gordon *et al.*[19] who mentioned that the formal charges N(+) and S(−) suggested by structures **4**–**4**‴ are in line with the differences between the electronegativities of nitrogen and sulfur (quoted as 3.0 and 2.8, respectively), and who reported negative natural and Mulliken charges for nitrogen and positive natural and Mulliken charges for sulfur, in agreement with earlier findings[7,12].

The comparison between the vertical cuts through the isotropic shielding surrounding the S–N and

C–C bonds in the electronic ground states of S_2N_2 and benzene (see Figure 3) shows that the C–C bond is more shielded and its shielded area extends over larger distances above and below the molecular plane. Looking at the S–N bond, the isotropic shielding decreases quickly in directions perpendicular to the molecular plane above and below the sulfur atom, becoming lower than 15 ppm at distances of just about 0.4 Å. The shapes and density of the contours surrounding the nitrogen atom suggest that this atom is the main contributor to the S–N bond, especially in the regions above and below the molecular plane. According to these observations, the S–N bond is noticeably weaker than the C–C bond and the π character of this bond is associated mainly with the nitrogen atom. This provides further arguments in favour of models **1** and **4**–**4**‴ from the Introduction. The $\sigma_{\rm iso}(\mathbf{r})$ contours on both sides of the S–N bond in Figure 3(a) indicate that the lone pairs on these atoms make similar relatively minor contributions to the isotropic shielding in the vertical plane cutting through the bond, but are more pronounced around the sulfur atoms.

The shapes of the $\sigma_{\rm iso}(\mathbf{r})$ contour plots for the electronic ground state of S_2N_2 in vertical planes passing through the two sulfur and two nitrogen atoms (see Figure 4) reinforce the conclusion that the contributions of the nitrogen atoms to the π system are more significant than those of the sulfur atoms. None of the contour plots in Figure 4 suggests a diagonal bonding interaction between the pair of nitrogen atoms or between the pair of sulfur atoms. The $\sigma_{\rm iso}(\mathbf{r})$ contours in Figure 4 show that the lone pairs on the sulfur atoms make more substantial contributions to the isotropic shielding outside the ring, in line with similar observations mentioned above in relation to Figures 1(a) and 3(a).

The contour plots in Figures 1, 3 and 4 show that $\sigma_{\rm iso}(\mathbf{r})$ changes very quickly in the close neighbourhood of a nucleus. This is particularly noticeable around the sulfur atoms: On approaching one of these atoms from the ring centre, $\sigma_{\rm iso}(\mathbf{r})$ increases to values above 180 ppm over a very short distance, then abruptly drops down to negative values below –128 ppm and then increases again before the nucleus in reached, at which $\sigma_{\rm iso}(^{33}{\rm S}) = -77.79$ ppm (see Table 2). The nitrogen atoms are surrounded by strongly deshielded regions, in parts of which $\sigma_{\rm iso}(\mathbf{r})$ decreases to under –215 ppm.

The isotropic shielding contour plots for the S_1 and T_1 electronic states of S_2N_2 (corresponding to vertical excitations from S_0) shown in Figures 5–9 depict $\sigma_{\rm iso}(\mathbf{r})$ behaviour which is very different from that in the electronic ground state. The S_1 and T_1 electronic states of S_2N_2 both feature sizeable deshielded regions spreading out in all directions from the ring centre. The deshielded region in the T_1 electronic state of S_2N_2 is very similar in shape and extent to the deshielded regions observed in the ground electronic state of square cyclobutadiene and in the S_1 and T_1 electronic states of benzene, where these deshielded regions were shown to be the driving force behind aromatic destabilization[41]. As can easily be seen in Figure 5(b), the extensive deshielded region in the centre of the ring reduces the sizes and intensities of the shielded regions corresponding to individual S–N bonds and it displaces

Place Figures 5–9 near here.

their more shielded parts to off-bond locations outside the ring. A comparison to the electronic ground state shielding picture in Figure 1(a) shows clearly that the S–N bonds in T_1 are much weaker. This observation is reinforced by the comparison between Figures 3(a) and 7(b). A key conclusion that arises from this analysis of the isotropic shielding distribution in the T_1 electronic state of S_2N_2 is that this state is antiaromatic with much weaker but still easily discernible S–N bonds which should be sufficient for maintaining the ring structure. However, the T_1 electronic state is likely to assume a lower-energy geometry, with a symmetry lower than that of the electronic ground state geometry. It has been argued that the T_1 ($1\,^3B_{3u}$) state of S_2N_2 is involved in the polymerization mechanism of S_2N_2 to $(SN)_x$ [26]; such involvement could of course be facilitated by the weakened ring structure revealed by the current shielding analysis.

The isotropic shielding contour plots for the S_1 electronic state of S_2N_2 (see the left panels in Figures 5–9) show that the surprisingly large NICS(0) and NICS(1) values for this state that were reported in Table 3 correspond to locations which are surrounded by an extensive strongly deshielded region originating at the ring centre. The NICS data in Table 3 suggests that the extent of deshielding within this region is exaggerated by calculations in the cc-pVTZ basis, but that it would remain much more extensive and deshielded than the corresponding region in the T_1 electronic state even if the isotropic shielding contour plots were calculated in a much larger basis, such as aug-cc-pVQZ. The extensive central deshielded region in the S_1 electronic state of S_2N_2 completely obliterates the S–N bonds. As a consequence, the S_1 state of S_2N_2 can be expected to be highly unstable, given that there are no obvious interactions that would keep the atoms together.

Conclusions

The magnetic properties of the low-lying electronic states of S_2N_2 studied in this paper strongly suggest that the electronic ground state of this four-membered ring is aromatic, but less so than is the electronic ground state of benzene, that the lowest singlet excited state is profoundly antiaromatic at the same geometry, to an extent that removes any bonding interactions that would keep the atoms together, and that the lowest triplet state is also antiaromatic, but its antiaromaticity is more moderate and similar to that observed in the electronic ground state of square cyclobutadiene. In this way, S_2N_2 becomes the first example of an inorganic ring for which theory predicts substantial changes in aromaticity upon transition from the ground state to the first singlet excited or lowest triplet electronic states.

The first singlet excited and lowest triplet electronic states of S_2N_2 were confirmed as $1\,^1A_u$ and $1\,^3B_{3u}$, respectively, through linear response CC3/aug-cc-pVTZ calculations of the vertical excitation energies from the ground electronic state to the next eight singlet electronic states and to the eight lowest triplet states. These calculations provide the most accurate theoretical estimates of these excitation

energies that are available to date.

Two aromaticity indices, NICS(0) and NICS(0)$_{zz}$, fail to provide reliable assessments of the aromaticity of the electronic ground state of S_2N_2. The value of NICS(0) reflects the presence of a small deshielded region in the centre of the ring, a minor feature which could be due to the presence of a weak σ electron antiaromatic system competing with the aromatic system formed by the π electrons. The NICS(0)$_{zz}$ index is also unreliable as a measure of the aromaticity in this system because of the high shielding anisotropy at the centre of the ring; the current results suggest that the use of this index should be avoided in such situations. On the other hand, the NICS(1) and NICS(1)$_{zz}$ indices, which are influenced mainly by the π electrons, the isotropic magnetic susceptibility, $\chi_{\rm iso}$, and the out-of-plane component of the magnetic susceptibility tensor, χ_{zz}, have no problems with identifying the electronic ground state of S_2N_2 as moderately aromatic. All NICS indices, $\chi_{\rm iso}$ and χ_{zz} agree on the levels of antiaromaticity of the first singlet excited and the lowest triplet electronic states of S_2N_2.

The analysis of the behaviour of the isotropic magnetic shielding, $\sigma_{\rm iso}(\mathbf{r})$, within the space surrounding the molecular framework for the ground, first singlet excited and lowest triplet electronic states of S_2N_2 provides a detailed account of the substantial differences between the chemical bonding features and aromaticies of these states.

The doughnut-shaped region of increased shielding enclosing the carbon ring in the electronic ground state of benzene, which is indicative of strong bonding interactions and aromatic stability, is also observed, in reduced size, in the electronic ground state of S_2N_2. This size reduction affects mainly the height and depth of the S_2N_2 shielded "doughnut" above and below the molecular plane, which suggests that the π bond component in the S–N bond in S_2N_2 is weaker than its counterpart in the C–C bond in benzene. The $\sigma_{\rm iso}(\mathbf{r})$ contour plots for the electronic ground state of S_2N_2 show that the more intensively shielded regions above and below the molecular plane are primarily above and below the nitrogen atoms, whereas the regions above and below the sulfur atoms are significantly less shielded. This is an indication that most of the π electron activity is focused around the nitrogen atoms; the nitrogen atoms are also found to be the main contributors to the S–N bonds. These observations are consistent with the 6π-electron models for the electronic structure of S_2N_2 which place at least one π electron pair on a nitrogen atom, **1** and the sequence **4**–**4**$'''$ (see the Introduction). The current isotropic magnetic shielding analysis shows no hints of diagonal bonding interactions of the types depicted in models **1** and **3**. While we have not sought direct evidence of the singlet diradical character of the electronic ground state of S_2N_2, this is the most likely reason for the large deviations of magnetic properties calculated with the HF-GIAO and MP2-GIAO methods from their CASSCF-GIAO, CCSD(T)-GIAO and CCSDT-GIAO counterparts.

The isotropic magnetic shielding picture of the lowest triplet electronic state of S_2N_2 follows the

antiaromatic pattern familiar from the electronic ground state of square cyclobutadiene and the lowest triplet electronic state of benzene[41], featuring a strongly deshielded dumbbell-shaped region in the centre of the molecule, which weakens the bonds forming the ring. A deshielded dumbbell-shaped region in the centre of the molecule is also observed in the lowest singlet excited electronic state of S_2N_2 but its hitherto unprecedented extent and intensity suggest that the molecule would immediately dissociate following vertical excitation to this state.

Conflict of interest

The authors declare no conflict of interest.

Acknowledgments

M. A. H. Al-Yassiri thanks the Higher Committee for Education Development in Iraq (HCED Iraq) for sponsoring his scholarship at the University of York.

Keywords: disulfur dinitride · bonding in S_2N_2 · aromaticity of S_2N_2 · excited-state aromaticity · ^{33}S isotropic magnetic shielding · ^{15}N isotropic magnetic shielding · nucleus-independent chemical shifts · magnetic susceptibilities

[1] F. P. Burt, *J. Chem. Soc.* **1910**, *97*, 1171–1174.

[2] M. Goehring, Voigt, D., *Naturwissenschaften* **1953**, *40*, 482.

[3] V. V. Walatka Jr., M. M. Labes, J. H. Perlstein, *Phys. Rev. Lett.* **1973**, *31*, 1139–1142.

[4] F. E. Penotti, D. L. Cooper, P. B. Karadakov, *to be published*.

[5] R. L. Greene, G. B. Street, L. J. Suter, *Phys. Rev. Lett.* **1975**, *34*, 577–579.

[6] C. Edmiston, K. Ruedenberg, *Rev. Mod. Phys.* **1963**, *35*, 457–465.

[7] R. R. Adkins, A. G. Turner, *J. Am. Chem. Soc.* **1978**, *100*, 1383–1387.

[8] N. Greenwood, A. Earnshaw, *Chemistry of the Elements* (Pergamon Press, Oxford, 1984).

[9] R. H. Findlay, M. H. Palmer, A. J. Downs, R. G. Egdell, R. Evans, *Inorg. Chem.* **1980**, *19*, 1307–1314.

[10] J. M. Foster, S. F. Boys, *Rev. Mod. Phys.* **1960**, *32*, 300–302.

[11] H. Fujimoto, T. Yokoyama, *Bull. Chem. Soc. Jpn.* **1980**, *53*, 800.

[12] J. Gerratt, S. J. McNicholas, P. B. Karadakov, M. Sironi, M. Raimondi, D. L. Cooper, *J. Am. Chem. Soc.* **1996**, *118* 6472–6476.

[13] R. D. Harcourt, *ChemPhysChem* **2013**, *14*, 2859–2864.

[14] T. Thorsteinsson, D. L. Cooper, *J. Math. Chem.* **1998**, *23*, 105–126.

[15] B. Braïda, A. Lo, P. C. Hiberty, *ChemPhysChem* **2012**, *13*, 811–819.

[16] B. H. Chirgwin, C. A. Coulson, *Proc. Roy. Soc. Lond. Ser. A* **1950**, *201*, 196–209.

[17] T. Thorsteinsson, D. L. Cooper, J. Gerratt, M. Raimondi, *Molec. Eng.* **1997**, *7*, 67–85.

[18] H. M. Tuononen, R. Suontamo, J. Valkonen, R. S. Laitinen, *J. Phys. Chem. A* **2004**, *108*, 5670–5677.

[19] Y. Jung, T. Heine, P. v. R. Schleyer, M. Head-Gordon, *J. Am. Chem. Soc.* **2004**, *126*, 3132–3138.

[20] H. M. Tuononen, R. Suontamo, J. Valkonen, R. S. Laitinen, T. Chivers, *J. Phys. Chem. A* **2005**, *109*, 6309–6317.

[21] E. F. Hayes, A. K. Q. Siu, *J. Amer. Chem. Soc.* **1971**, *93*, 2090–20191.

[22] W. D. Laidig, H. F. Schaefer, *J. Chem. Phys.* **1981**, *74*, 3411–3414.

[23] P. v. R. Schleyer, M. Manoharan, Z.-X. Wang, B. Kiran, H. Jiao, R. Puchta, N. J. R. v. E. Hommes, *Org. Lett.* **2001**, *3*, 2465–2468.

[24] T. Heine, P. v. R. Schleyer, C. Corminboeuf, G. Seifert, R. Reviakine, J. Weber, *J. Phys. Chem. A* **2003**, *107*, 6470–6475.

[25] J. A. Jafri, M. D. Newton, T. A. Pakkanen, J. L. Whitten, *J. Chem. Phys.***1977**, *66*, 5167–5172.

[26] M. H. Palmer, M. F. Guest, *Chem. Phys.* **1986**, *110*, 187–194.

[27] A. J. Bridgeman, B. Cunningham, *Spectrochim. Acta A* **2004**, *60*, 471–480.

[28] P. B. Karadakov, K. E. Horner, *J. Chem. Theory Comput.* **2016**, *12*, 558–563.

[29] P. B. Karadakov, J. Kirsopp, *Chem. Eur. J.* **2017**, *23*, 12949–12954.

[30] P. B. Karadakov, K. E. Horner, *J. Phys. Chem. A* **2013**, *117*, 518–523.

[31] C. Foroutan-Nejad, S. Shahbazian, F. Feixas, P, Rashidi-Ranjbar, Miquel Solà, *J. Comput. Chem.* **2011**, *32*, 2422–2431.

[32] C. Foroutan-Nejad, *Theor. Chem. Acc.* **2015**, *134:8*, 1–9.

[33] S. Fias, P. W. Fowler, J. L. Delgado, U. Hahn, P. Bultinck, *Chem. Eur. J.* **2008**, *14*, 3093–3099.

[34] S. Van Damme, G. Acke, R. W. A. Havenith, P. Bultinck, *Phys. Chem. Chem. Phys.* **2016**, *18*, 11746–11755.

[35] M. Rosenberg, C. Dahlstrand, K. Kilså, H. Ottosson, *Chem. Rev.* **2014**, *114*, 5379–5425.

[36] Y. M. Sung, M.-C. Yoon, J. M. Lim, H. Rath, K. Naoda, A. Osuka, D. Kim, *Nature Chem.* **2015**, *7*, 418–422.

[37] Y. M. Sung, J. Oh, W. Kim, H. Mori, A. Osuka, D. Kim, *J. Am. Chem. Soc.* **2015**, *137*, 11856–11859.

[38] N. C. Baird, *J. Am. Chem. Soc.* **1972**, *94*, 4941–4948.

[39] P. B. Karadakov, *J. Phys. Chem. A* **2008**, *112*, 7303–7309.

[40] P. B. Karadakov, *J. Phys. Chem. A* **2008**, *112*, 12707–12713.

[41] P. B. Karadakov, P. Hearnshaw, K. E. Horner, *J. Org. Chem.* **2015**, *81*, 11346–11352.

[42] A. Perrin, A. F. Antognini, X. Zeng, H. Beckers, H. Willner, G. Rauhut, *Chem. Eur. J.* **2014**, *20*, 10323–10331.

[43] V. Gogonea, P. v. R. Schleyer, P. R. Schreiner, *Angew. Chem. Int. Ed.*, *37*, 1945–1948.

[44] P. W. Fowler, E. Steiner, L. W. Jenneskens, *Chem. Phys. Lett.* **2003**, *371*, 719–723.

[45] Z. Rinkevicius, J. Vaara, L. Telyatnyk, O. Vahtras, *J. Chem. Phys.* **2003**, *118*, 2550–2561.

[46] J. Vaara, *Phys. Chem. Chem. Phys.* **2007**, *9*, 5399–5418.

[47] B. O. Roos, K. Andersson, M. P. Fülscher, *Chem. Phys. Lett* **1992**, *192*, 5–13.

[48] O. Christiansen, H. Koch, A. Halkier, P. Jørgensen, T. Helgaker, A. S. de Merás, *J. Chem. Phys.* **1996**, *105*, 6921–6939.

[49] K. Halda, C. Hättig, P. Jørgensen,. *J. Chem. Phys.* **2000**, *13*, 7765–7772.

[50] K. Ruud, T. Helgaker, R. Kobayashi, P. Jørgensen, K. L. Bak, H. J. A. Jensen, *J. Chem. Phys.* **1994**, *100*, 8178–8185.

[51] K. Ruud, T. Helgaker, K. L. Bak, P. Jørgensen, J. Olsen, *Chem. Phys.* **1995**, *195*, 157–169.

[52] K. Aidas, C. Angeli, K. L. Bak, V. Bakken, R. Bast, L. Boman, O. Christiansen, R. Cimiraglia, S. Coriani, P. Dahle, E. K. Dalskov, U. Ekström, T. Enevoldsen, J. J. Eriksen, P. Ettenhuber, B. Fernández, L. Ferrighi, H. Fliegl, L. Frediani, K. Hald, A. Halkier, C. Hättig, H. Heiberg, T. Helgaker, A. C. Hennum, H. Hettema, R. Hjertenæs, S. Høst, I.-M. Høyvik, M. F. Iozzi, B. Jansík, H. J. Aa. Jensen, D. Jonsson, P. Jørgensen, J. Kauczor, S. Kirpekar, T. Kjærgaard, W. Klopper, S. Knecht, R. Kobayashi, H. Koch, J. Kongsted, A. Krapp, K. Kristensen, A. Ligabue, O. B. Lutnæs, J. I. Melo, K. V. Mikkelsen, R. H. Myhre, C. Neiss, C. B. Nielsen, P. Norman, J. Olsen, J. M. H. Olsen, A. Osted, M. J. Packer, F. Pawlowski, T. B. Pedersen, P. F. Provasi, S. Reine, Z. Rinkevicius, T. A. Ruden, K. Ruud, V. V. Rybkin, P. Sałek, C. C. M. Samson, A. Sánchez de Merás, T. Saue, S. P. A. Sauer, B. Schimmelpfennig, K. Sneskov, A. H. Steindal, K. O. Sylvester-Hvid, P. R. Taylor, A. M. Teale, E. I. Tellgren, D. P. Tew, A. J. Thorvaldsen, L. Thøgersen, O. Vahtras, M. A. Watson, D. J. D. Wilson, M. Ziolkowski, H. Ågren, *WIREs Comput. Mol. Sci.* **2014**, *4*, 269–284; *Dalton, a Molecular Electronic Structure Program, Release Dalton2016.2*, **2016**, see http://daltonprogram.org.

[53] J. F. Stanton, J. Gauss, M. E. Harding, P. G. Szalay, with contributions from A. A. Auer, R. J. Bartlett, U. Benedikt, C. Berger, D. E. Bernholdt, Y. J. Bomble, L. Cheng, O. Christiansen O., M. Heckert, O. Heun, C. Huber, T.-C. Jagau, D. Jonsson, J. Jusélius, K. Klein, W. J. Lauderdale, D. A. Matthews, T. Metzroth, L. A. Mück, D. P. O'Neill, D. R. Price, E. Prochnow, C. Puzzarini, K. Ruud, F. Schiffmann, W. Schwalbach, C. Simmons, S. Stopkowicz, A. Tajti, J. Vázquez, F. Wang, J. D. Watts, and the integral packages MOLECULE (J. Almlöf, P. R. Taylor), PROPS (P. R. Taylor), ABACUS (T. Helgaker, H. J. Aa. Jensen, P. Jørgensen, J. Olsen,), and ECP routines by A. V. Mitin, C. van Wüllen, *CFOUR, Coupled-Cluster Techniques for Computational Chemistry, a Quantum-Chemical Program Package*, see http://www.cfour.de.

[54] P. v. R. Schleyer, C. Maerker, A. Dransfeld, H. Jiao, N. J. R. v. E. Hommes, *J. Am. Chem. Soc.* **1996**, *118*, 6317–6318.

[55] I. Cernusak, P W. Fowler, E. Steiner, *Mol. Phys.* **2000**, *98*, 945–953.

[56] E. Steiner, P. W. Fowler, L. W. Jenneskens, *Angew. Chem. Int. Ed.* **2001**, *40*, 362–366.

[57] P. v. R. Schleyer, H. Jiao, N. J. R. v. E. Hommes, V. G. Malkin, O. L.Malkina, *J. Am. Chem. Soc.* **1997**, *119*, 12669–12670.

[58] H. Fallah-Bagher-Shaidaei, C. S. Wannere, C. Corminboeuf, R. Puchta, P. v. R. Schleyer, *Org. Lett.* **2006**, *8*, 863–866.

Tables and Figures

Table 1. Vertical excitation energies (in eV) from S_0 to the next eight singlet (S_1–S_8) and the eight lowest triplet (T_1–T_8) electronic states of S_2N_2 calculated at different levels of theory. Number of the state corresponding to energy ordering for a particular method in brackets. CASSCF corresponds to CASSCF(22,16). For further details, see text.

Method/Singlet State	$2\,^1A_g$	$1\,^1B_{3u}$	$1\,^1B_{2u}$	$1\,^1B_{1g}$	$1\,^1B_{1u}$	$1\,^1B_{2g}$	$1\,^1B_{3g}$	$1\,^1A_u$
CASSCF/cc-pVTZ	5.57(4)	6.13(5)	6.26(6)	6.93(8)	4.96(1)	5.12(3)	6.75(7)	5.11(2)
CASSCF/aug-cc-pVTZ	5.54(4)	6.09(5)	6.23(6)	6.90(8)	4.93(1)	5.12(3)	6.72(7)	5.05(2)
CCSD/cc-pVTZ	5.26(4)	5.73(6)	5.40(5)	6.21(8)	4.74(3)	4.66(2)	5.99(7)	4.50(1)
CCSD/aug-cc-pVTZ	5.21(4)	5.64(6)	5.31(5)	6.13(8)	4.71(3)	4.65(2)	5.93(7)	4.42(1)
CCSDR(3)/cc-pVTZ	5.05(4)	5.56(6)	5.33(5)	6.08(8)	4.61(2)	4.68(3)	6.00(7)	4.46(1)
CCSDR(3)/cc-pVQZ	5.00(4)	5.49(6)	5.25(5)	6.00(8)	4.58(2)	4.65(3)	5.94(7)	4.36(1)
CCSDR(3)/aug-cc-pVTZ	5.00(4)	5.48(6)	5.24(5)	6.00(8)	4.58(2)	4.66(3)	5.93(7)	4.37(1)
CCSDR(3)/aug-cc-pVQZ	4.98(4)	5.46(6)	5.21(5)	5.97(8)	4.57(2)	4.64(3)	5.91(7)	4.33(1)
CC3/cc-pVTZ	4.96(4)	5.49(6)	5.27(5)	6.02(8)	4.54(2)	4.62(3)	5.94(7)	4.43(1)
CC3/aug-cc-pVTZ	4.90(4)	5.41(6)	5.18(5)	5.94(8)	4.50(2)	4.60(3)	5.88(7)	4.33(1)
Method/Triplet State	$1\,^3A_g$	$1\,^3B_{3u}$	$1\,^3B_{2u}$	$1\,^3B_{1g}$	$1\,^3B_{1u}$	$1\,^3B_{2g}$	$1\,^3B_{3g}$	$1\,^3A_u$
CASSCF/cc-pVTZ	5.25(6)	3.28(1)	4.32(2)	5.94(7)	4.65(5)	4.61(4)	6.17(8)	4.48(3)
CASSCF/aug-cc-pVTZ	5.23(6)	3.29(1)	4.27(2)	5.91(7)	4.63(5)	4.62(4)	6.14(8)	4.44(3)
CCSD/cc-pVTZ	4.94(6)	3.03(1)	3.58(2)	5.39(8)	4.42(5)	4.11(4)	5.37(7)	4.01(3)
CCSD/aug-cc-pVTZ	4.90(6)	3.06(1)	3.51(2)	5.33(8)	4.40(5)	4.10(4)	5.31(7)	3.95(3)
CC3/cc-pVTZ	4.69(6)	3.17(1)	3.67(2)	5.27(7)	4.25(5)	4.12(4)	5.38(8)	3.97(3)
CC3/aug-cc-pVTZ	4.64(6)	3.20(1)	3.60(2)	5.21(7)	4.23(5)	4.11(4)	5.32(8)	3.90(3)

Table 2. Sulfur and nitrogen isotropic shieldings in the S_0, S_1 and T_1 electronic states of S_2N_2, carbon and proton isotropic shieldings in the electronic ground state of benzene (in ppm), and corresponding magnetic susceptibilities (in ppm cm^3 mol^{-1}). CASSCF(22,16) for S_2N_2 and CASSCF(6,6) for benzene. For further details, see text.

S_2N_2	Method	$\sigma_{iso}(^{33}S)$	$\sigma_{iso}(^{15}N)$	χ_{iso}	χ_{zz}
S_0 ($1\,^1A_g$)	CASSCF-GIAO/cc-pVTZ	–77.79	–120.29	–29.37	–27.66
	CASSCF-GIAO/cc-pVQZ	–80.47	–125.62	–29.03	–27.37
	CASSCF-GIAO/aug-cc-pVTZ	–89.41	–120.09	–29.12	–27.45
	CASSCF-GIAO/aug-cc-pVQZ	–82.42	–126.33	–29.19	–28.16
	HF-GIAO/cc-pVTZ	–270.24	–285.05	–27.71	–35.04
	MP2-GIAO/cc-pVTZ	–55.18	–35.91	–27.19	–19.45
	CCSD(T)-GIAO/cc-pVTZ	–114.47	–124.38	–26.86	–24.16
	CCSDT-GIAO/cc-pVTZ	–117.23	–129.10	–26.86	–24.42
S_1 ($1\,^1A_u$)	CASSCF-GIAO/cc-pVTZ	–284.78	–151.83	163.27	494.46
	CASSCF-GIAO/cc-pVQZ	–429.02	–128.86	78.65	240.70
	CASSCF-GIAO/aug-cc-pVTZ	–433.74	–126.43	84.07	257.14
	CASSCF-GIAO/aug-cc-pVQZ	–445.19	–127.58	67.20	206.44
T_1 ($1\,^3B_{3u}$)	CASSCF-GIAO/cc-pVTZ	–227.96	9.58	–6.31	21.02
	CASSCF-GIAO/cc-pVQZ	–242.45	2.47	–5.42	22.06
	CASSCF-GIAO/aug-cc-pVTZ	–245.71	7.93	–5.58	22.13
	CASSCF-GIAO/aug-cc-pVQZ	–247.00	1.48	–4.84	23.08
C_6H_6	Method	$\sigma_{iso}(^{13}C)$	$\sigma_{iso}(^{1}H)$	χ_{iso}	χ_{zz}
S_0 ($1\,^1A_{1g}$)	CASSCF-GIAO/cc-pVTZ	73.44	24.96	–59.19	–99.70
S_0 ($1\,^1A_{1g}$)	CASSCF-GIAO/aug-cc-pVTZ	73.07	24.91	–59.11	–99.19

Table 3. NICS(0), NICS(0)$_{zz}$, NICS(1) and NICS(1)$_{zz}$ values in the S_0, S_1 and T_1 electronic states of S_2N_2, and in the electronic ground state of benzene (in ppm). CASSCF(22,16) for S_2N_2 and CASSCF(6,6) for benzene. For further details, see text.

S_2N_2	Method	NICS(0)	NICS(0)$_{zz}$	NICS(1)	NICS(1)$_{zz}$
S_0 ($1\,^1A_g$)	CASSCF-GIAO/cc-pVTZ	0.99	63.81	–2.64	–5.44
	CASSCF-GIAO/cc-pVQZ	1.08	62.33	–2.54	–6.11
	CASSCF-GIAO/aug-cc-pVTZ	1.41	63.72	–2.15	–5.60
	CASSCF-GIAO/aug-cc-pVQZ	1.23	62.39	–2.32	–6.05
	HF-GIAO/cc-pVTZ	–4.74	48.91	–5.09	-12.32
	MP2-GIAO/cc-pVTZ	5.60	73.01	–0.65	–0.16
	CCSD(T)-GIAO/cc-pVTZ	1.82	64.66	–1.95	–3.51
	CCSDT-GIAO/cc-pVTZ	1.66	64.18	–2.01	–3.70
S_1 ($1\,^1A_u$)	CASSCF-GIAO/cc-pVTZ	339.00	1004.56	313.03	926.19
	CASSCF-GIAO/cc-pVQZ	185.38	544.21	169.05	494.66
	CASSCF-GIAO/aug-cc-pVTZ	196.27	577.74	178.45	522.35
	CASSCF-GIAO/aug-cc-pVQZ	165.60	485.17	150.04	437.62
T_1 ($1\,^3B_{3u}$)	CASSCF-GIAO/cc-pVTZ	33.31	136.16	22.45	61.05
	CASSCF-GIAO/cc-pVQZ	33.45	135.35	22.94	61.05
	CASSCF-GIAO/aug-cc-pVTZ	34.14	137.41	23.36	62.44
	CASSCF-GIAO/aug-cc-pVQZ	33.77	135.89	23.20	62.34
C_6H_6	Method	NICS(0)	NICS(0)$_{zz}$	NICS(1)	NICS(1)$_{zz}$
S_0 ($1\,^1A_{1g}$)	CASSCF-GIAO/cc-pVTZ	–8.62	–12.63	–9.87	–27.71
S_0 ($1\,^1A_{1g}$)	CASSCF-GIAO/aug-cc-pVTZ	–8.32	–12.58	–9.43	–27.76

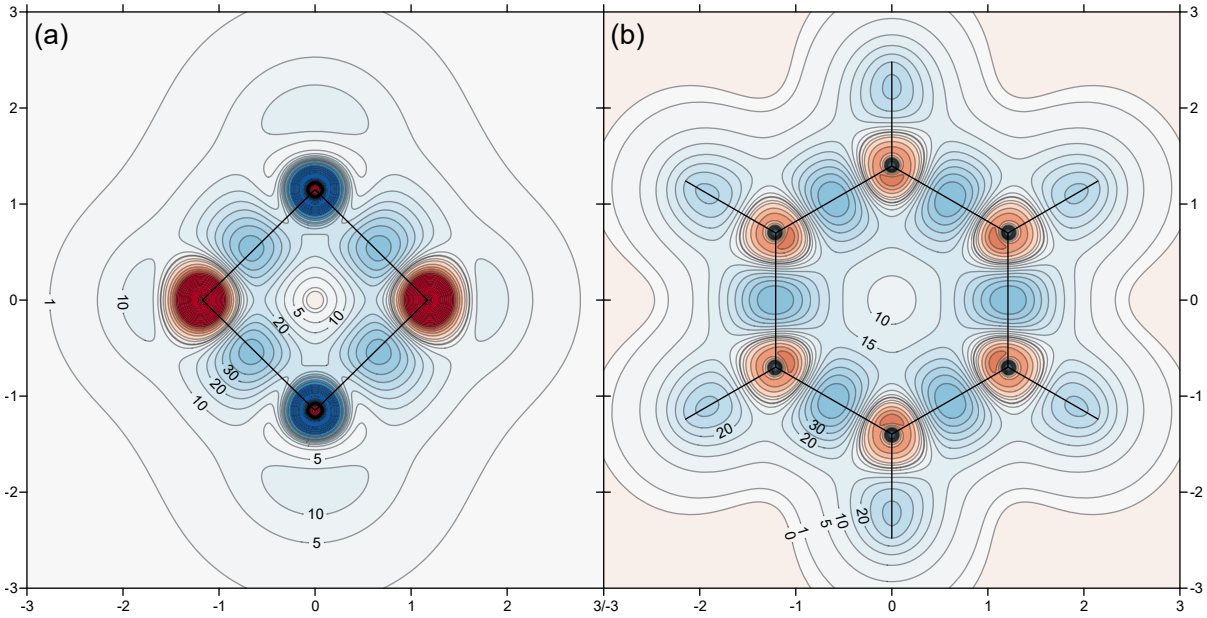

Figure 1. Isotropic shielding contour plots for the electronic ground states of (a) S_2N_2 and (b) benzene in the respective molecular (horizontal) planes. Contour levels, red (deshielded) to blue (shielded), between (a) -200 to 180, (b) -40 to 60; $\sigma_{\mathrm{iso}}(\mathbf{r})$ in ppm, axes in Å. N atoms on the horizontal axis in (a).

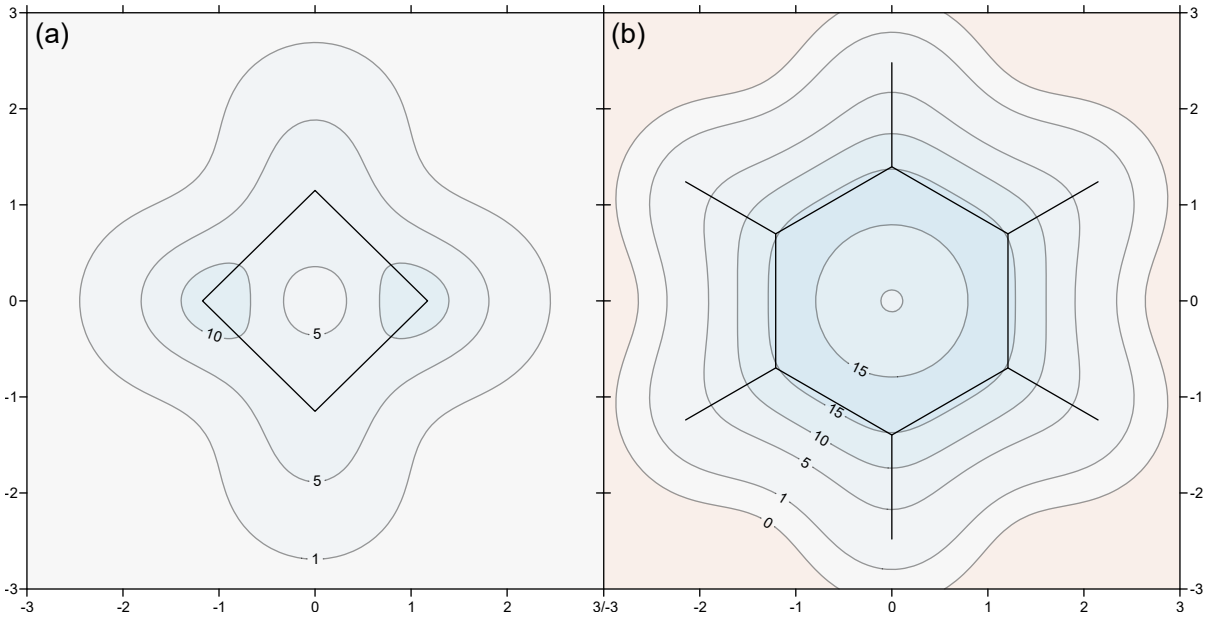

Figure 2. Isotropic shielding contour plots for the electronic ground states of (a) S_2N_2 and (b) benzene in planes parallel to and 1 Å above the respective molecular planes. Contour levels, pink (slightly deshielded) to blue (shielded), between (a) 1 to 10, (b) 0 to 15; $\sigma_{\mathrm{iso}}(\mathbf{r})$ in ppm, axes in Å. N atoms on the horizontal axis in (a).

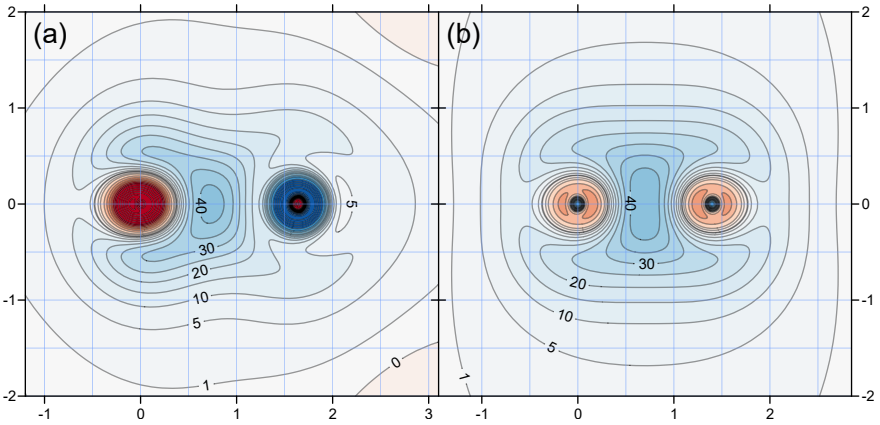

Figure 3. Isotropic shielding contour plots for the electronic ground states of (a) S_2N_2 and (b) benzene in vertical planes (perpendicular to the respective molecular planes) passing through the S–N and C–C bonds. N and S atoms in (a) at positions $(0, 0)$ and $(1.64182, 0)$, carbon atoms in (b) at positions $(0, 0)$ and $(1.3964, 0)$. Contour levels, red (deshielded) to blue (shielded), between (a) -200 to 160, (b) -30 to 60; $\sigma_{\text{iso}}(\mathbf{r})$ in ppm, axes and coordinates in Å.

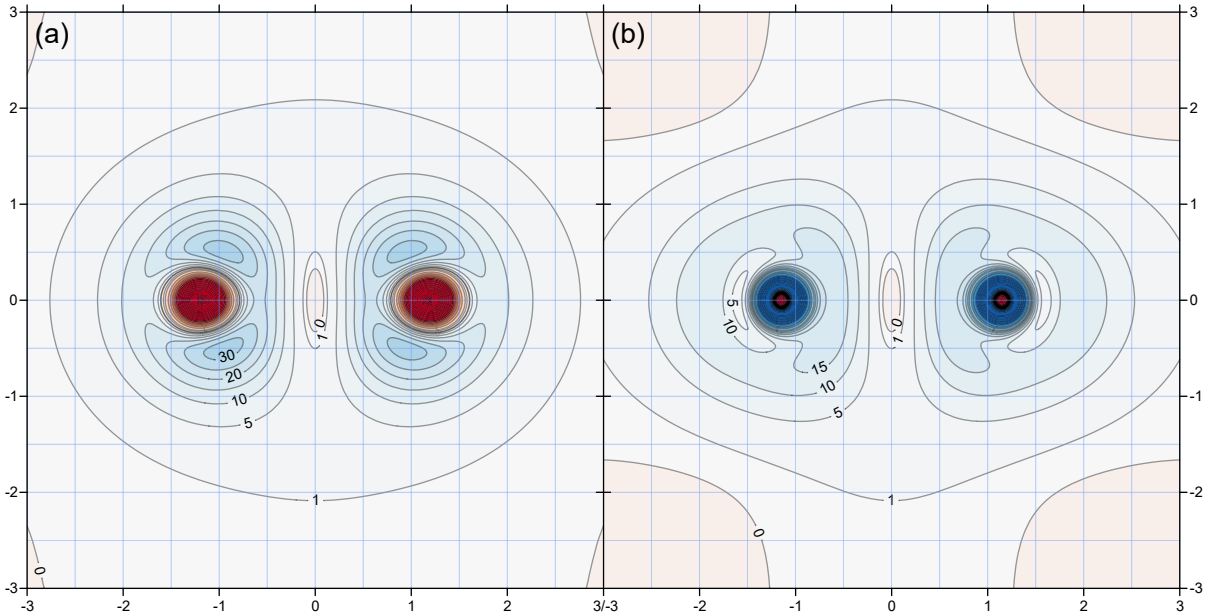

Figure 4. Isotropic shielding contour plots for the electronic ground state of S_2N_2 in vertical planes (perpendicular to the molecular plane) passing through (a) the two nitrogen atoms and (b) the two sulfur atoms. N atoms in (a) at positions $(\pm 1.171748, 0.0)$, S atoms in (b) at positions $(\pm 1.150035, 0.0)$. Contour levels, red (deshielded) to blue (shielded), between (a) -200 to 30, (b) -120 to 180; $\sigma_{\text{iso}}(\mathbf{r})$ in ppm, axes and coordinates in Å.

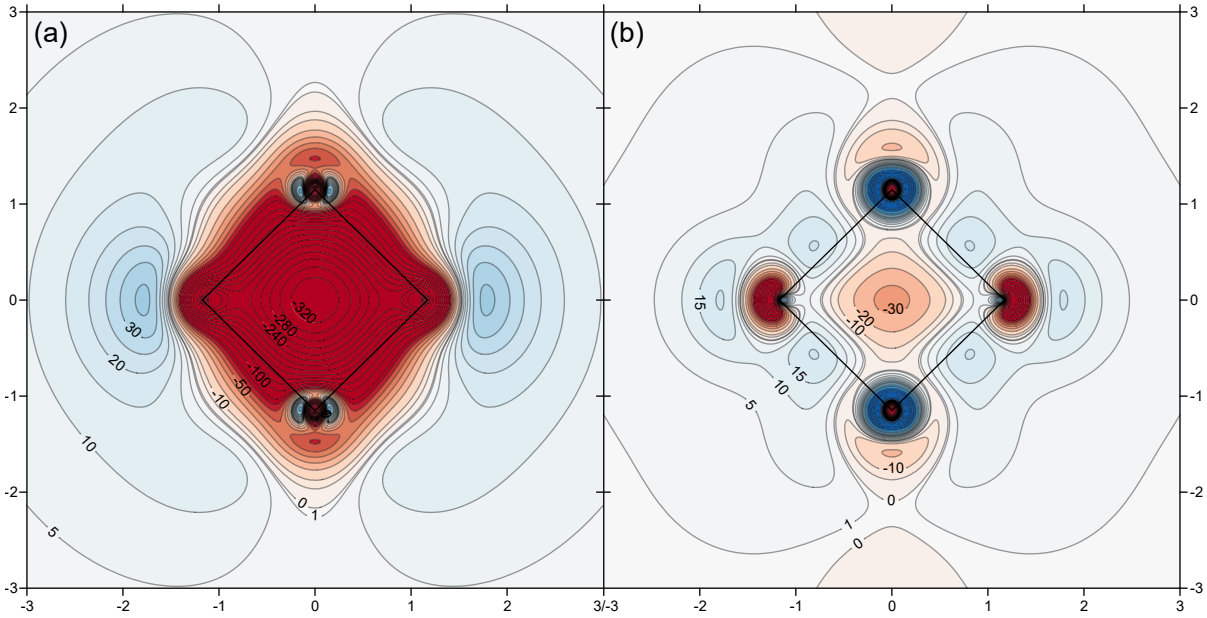

Figure 5. Isotropic shielding contour plots for the (a) S_1 and (b) T_1 electronic states of S_2N_2 in the molecular (horizontal) plane. Contour levels, red (deshielded) to blue (shielded), between (a) -480 to 50, (b) -260 to 180; $\sigma_{\mathrm{iso}}(\mathbf{r})$ in ppm, axes in Å. N atoms on the horizontal axis.

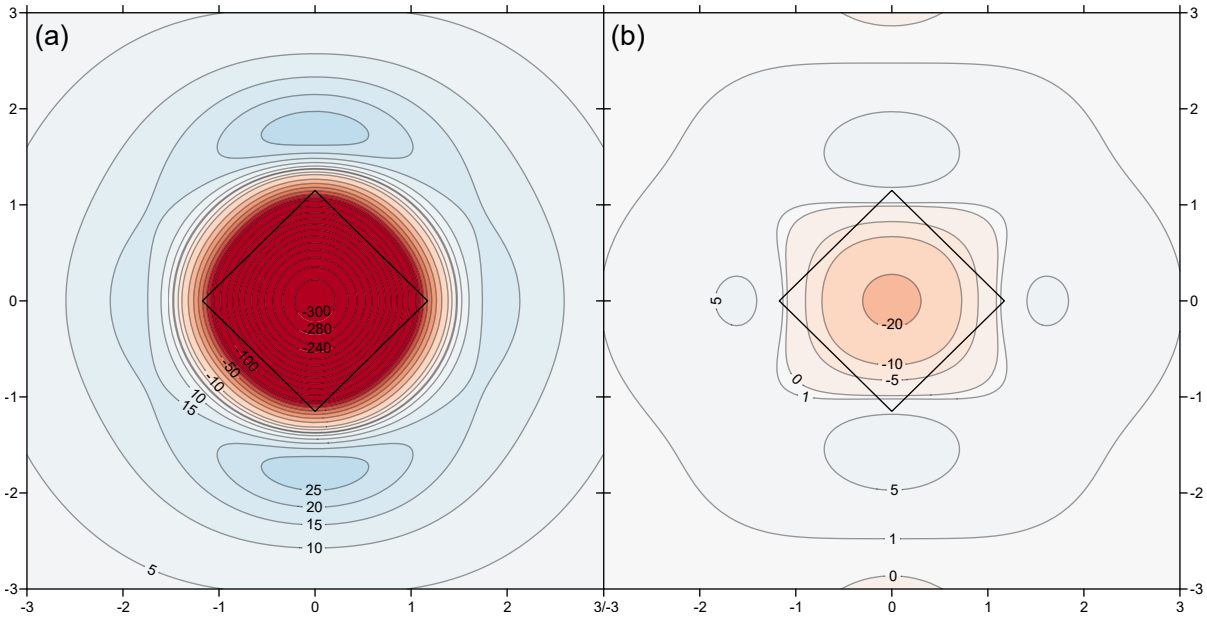

Figure 6. Isotropic shielding contour plots for the (a) S_1 and (b) T_1 electronic states of S_2N_2 in a plane parallel to and 1 Å above the molecular plane. Contour levels, red (deshielded) to blue (shielded), between (a) -300 to 25, (b) -20 to 5; $\sigma_{\mathrm{iso}}(\mathbf{r})$ in ppm, axes in Å. N atoms on the horizontal axis.

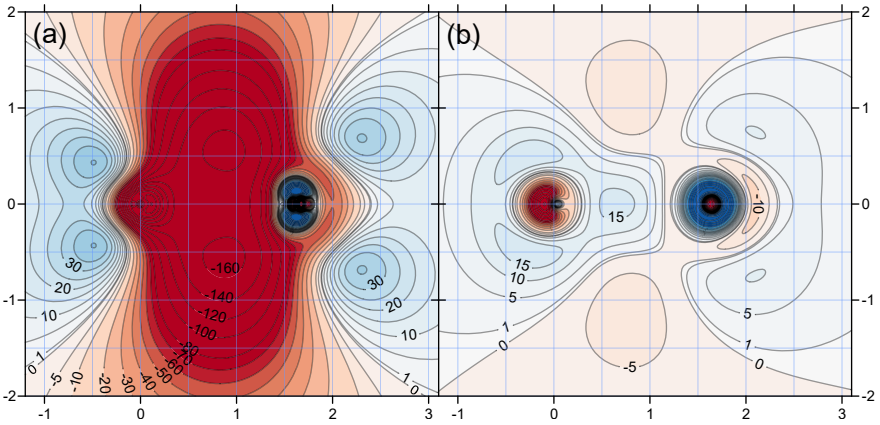

Figure 7. Isotropic shielding contour plots for the (a) S_1 and (b) T_1 electronic states of S_2N_2 in a vertical plane (perpendicular to the molecular plane) passing through the S–N bond. N and S atoms at positions $(0, 0)$ and $(1.64182, 0)$. Contour levels, red (deshielded) to blue (shielded), between (a) -800 to 260, (b) -260 to 140; $\sigma_{\text{iso}}(\mathbf{r})$ in ppm, axes and coordinates in Å.

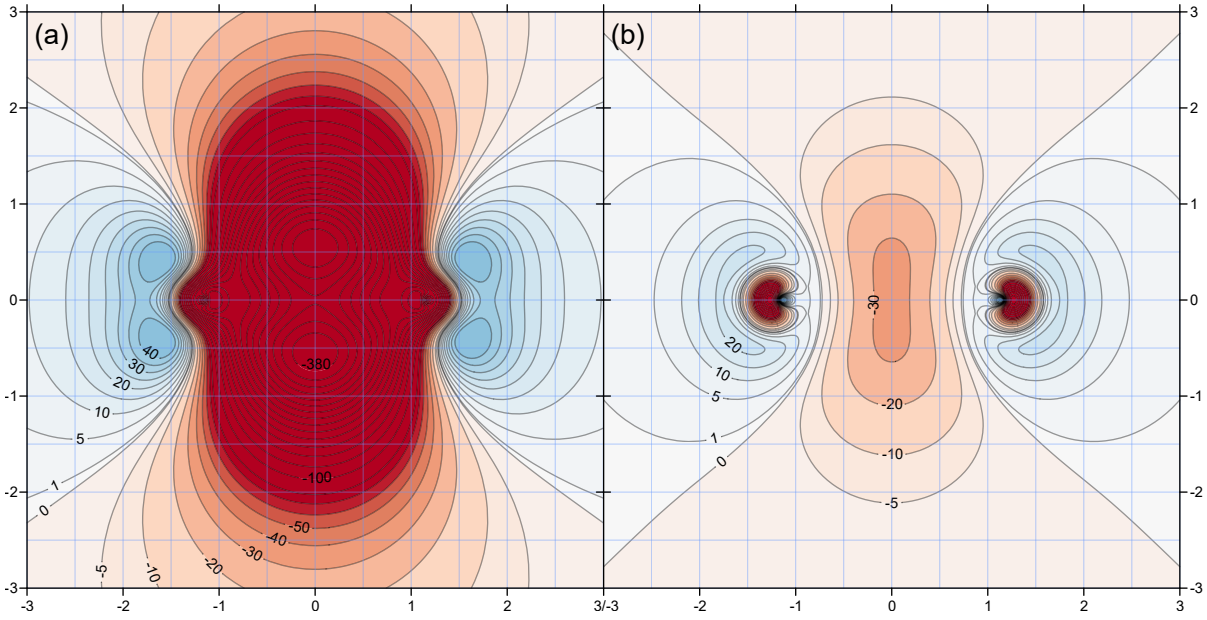

Figure 8. Isotropic shielding contour plots for the (a) S_1 and (b) T_1 electronic states of S_2N_2 in a vertical plane (perpendicular to the molecular plane) passing through the two nitrogen atoms, at positions $(\pm 1.171748, 0.0)$. Contour levels, red (deshielded) to blue (shielded), between (a) -380 to 40, (b) -200 to 60; $\sigma_{\text{iso}}(\mathbf{r})$ in ppm, axes and coordinates in Å.

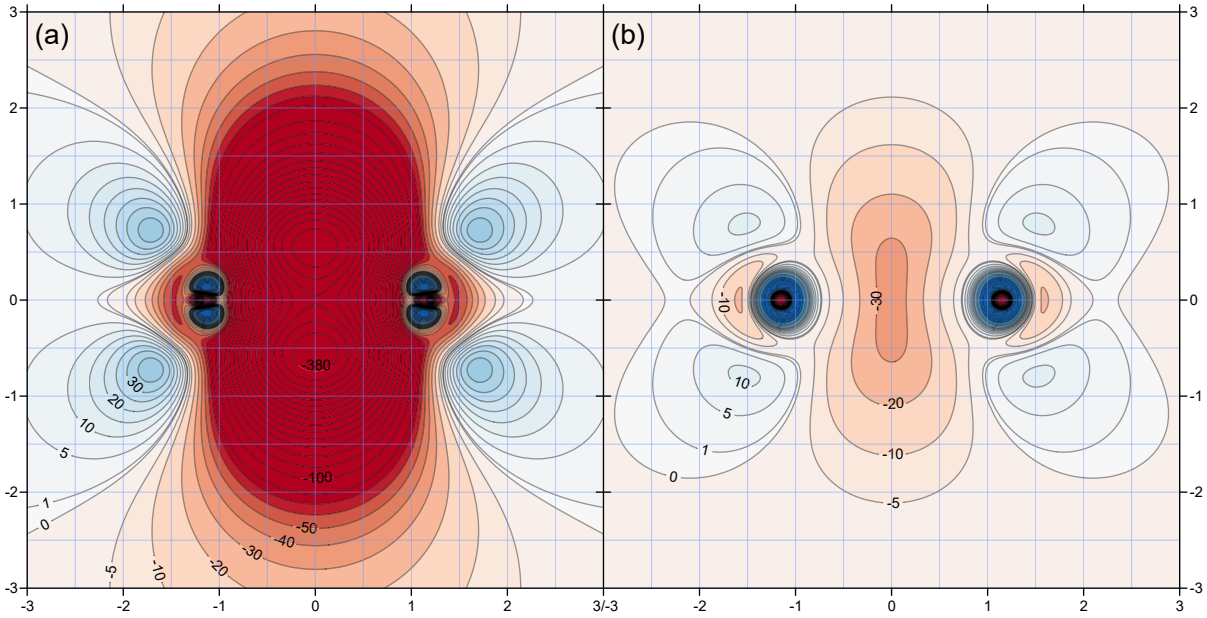

Figure 9. Isotropic shielding contour plots for the (a) S_1 and (b) T_1 electronic states of S_2N_2 in a vertical plane (perpendicular to the molecular plane) passing through the two sulfur atoms, at positions $(\pm 1.150035, 0.0)$. Contour levels, red (deshielded) to blue (shielded), between (a) -480 to 180, (b) -260 to 140; $\sigma_{\text{iso}}(\mathbf{r})$ in ppm, axes and coordinates in Å.

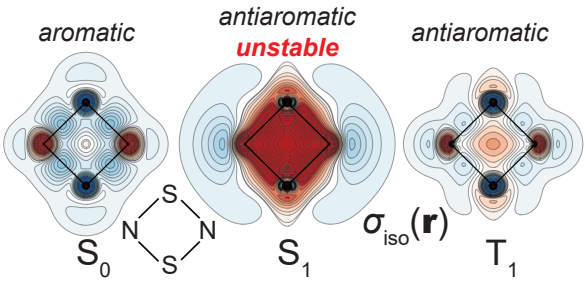

Is S_2N_2 aromatic? Off-nucleus shielding calculations strongly suggest that S_2N_2 is the first example of an inorganic ring showing substantial changes in aromaticity upon transition from the ground state (aromatic, but less so than is benzene) to the first singlet excited (strongly antiaromatic and unstable) or lowest triplet (antiaromatic) electronic states.